



**HAL**  
open science

# Expanded Parts Model for Semantic Description of Humans in Still Images

Gaurav Sharma, Frédéric Jurie, Cordelia Schmid

► **To cite this version:**

Gaurav Sharma, Frédéric Jurie, Cordelia Schmid. Expanded Parts Model for Semantic Description of Humans in Still Images. *IEEE Transactions on Pattern Analysis and Machine Intelligence*, 2017, 39 (1), pp.87-101. 10.1109/TPAMI.2016.2537325 . hal-01199160

**HAL Id: hal-01199160**

**<https://inria.hal.science/hal-01199160>**

Submitted on 20 Mar 2017

**HAL** is a multi-disciplinary open access archive for the deposit and dissemination of scientific research documents, whether they are published or not. The documents may come from teaching and research institutions in France or abroad, or from public or private research centers.

L'archive ouverte pluridisciplinaire **HAL**, est destinée au dépôt et à la diffusion de documents scientifiques de niveau recherche, publiés ou non, émanant des établissements d'enseignement et de recherche français ou étrangers, des laboratoires publics ou privés.

# Expanded Parts Model for Semantic Description of Humans in Still Images

Gaurav Sharma, *Member, IEEE*, Frédéric Jurie, and Cordelia Schmid, *Fellow, IEEE*

**Abstract**—We introduce an Expanded Parts Model (EPM) for recognizing human attributes (e.g. young, short hair, wearing suits) and actions (e.g. running, jumping) in still images. An EPM is a collection of part templates which are learnt discriminatively to explain specific scale-space regions in the images (in human centric coordinates). This is in contrast to current models which consist of a relatively few (i.e. a mixture of) ‘average’ templates. EPM uses only a subset of the parts to score an image and scores the image sparsely in space, i.e. it ignores redundant and random background in an image. To learn our model, we propose an algorithm which automatically mines parts and learns corresponding discriminative templates together with their respective locations from a large number of candidate parts. We validate our method on three recent challenging datasets of human attributes and actions. We obtain convincing qualitative and state-of-the-art quantitative results on the three datasets.

**Index Terms**—human analysis, attributes, actions, part-based model, mining, semantic description, image classification.

## 1 INTRODUCTION

THE focus of this paper is on semantically describing humans in still images using attributes and actions. It is natural to describe a person with attributes, e.g. age, gender, clothes, as well as with the action the person is performing, e.g. standing, running, playing a sport. We are thus interested in predicting such attributes and actions for human centric still images. While actions are usually dynamic, many of them are recognizable from a single static image, mostly due to the presence of (i) typical poses, like in the case of running and jumping, or (ii) a combination of pose, clothes and objects, like in the case of playing tennis or swimming.

With the incredibly fast growth of human centric data, e.g. on photo sharing and social networking websites or from surveillance cameras, analysis of humans in images is more important than ever. The capability to recognize human attributes and actions in still images could be used for numerous related applications, e.g. indexing and retrieving humans w.r.t. queries based on higher level semantic descriptions.

Human attributes and action recognition have been addressed mainly by (i) estimation of human pose [1], [2] or (ii) with general non-human-specific image classification methods [3], [4], [5], [6]. State-of-the-art action recognition performance has been achieved without solving the problem of pose estimation [1], [3], [5], [7], which is a challenging problem in itself. Concurrently, methods have been proposed to model interactions between humans and the object(s) associated with the actions [2], [8], [9], [10],

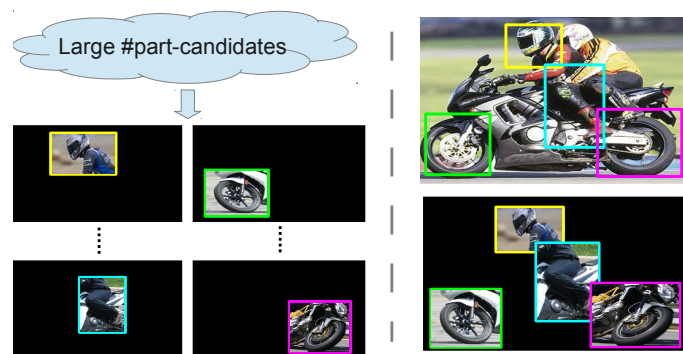


Fig. 1. Illustration of the proposed method. During training (left) discriminative templates are learnt from a large pool of randomly sampled part candidates. During testing (right), the most relevant parts are used to score the test image.

[11], [12]. In relevant cases, modelling interactions between humans and contextual objects is an interesting problem, but here we explore the broader and complementary approach of modeling appearance of humans and their immediate context for attribute and action recognition. When compared to methods exploiting human pose and human-object interactions, modelling appearance remains useful and complementary, while it becomes indispensable in the numerous other cases where there are no associated objects (e.g. actions like running, walking) and/or the pose is not immediately relevant (e.g. attributes like long hair, wearing a tee-shirt).

In this paper, we introduce a novel model for the task of semantic description of humans, the Expanded Parts Model (EPM). The input to an EPM is a human-centered image, i.e. it is assumed that the human positions in form of bounding boxes are available (e.g. from a human detection algorithm). An EPM is a collection of part templates, each of which can explain specific scale-space regions of an image. Fig. 1 illustrates learning and testing with EPM. In part based models the choice of parts is critical; it is not immediately

- Gaurav Sharma is with Max Planck Institute for Informatics, Germany. The majority of the work was done when he was with GREYC CNRS UMR 6072, Université de Caen Basse-Normandie, and INRIA-LEAR, France. <http://www.grosharma.com>
- Frédéric Jurie is with GREYC CNRS UMR 6072, Université de Caen Normandie, France. <http://jurie.users.greyc.fr>
- Cordelia Schmid is with LEAR, INRIA Grenoble Rhone Alpes, France. <http://lear.inrialpes.fr>

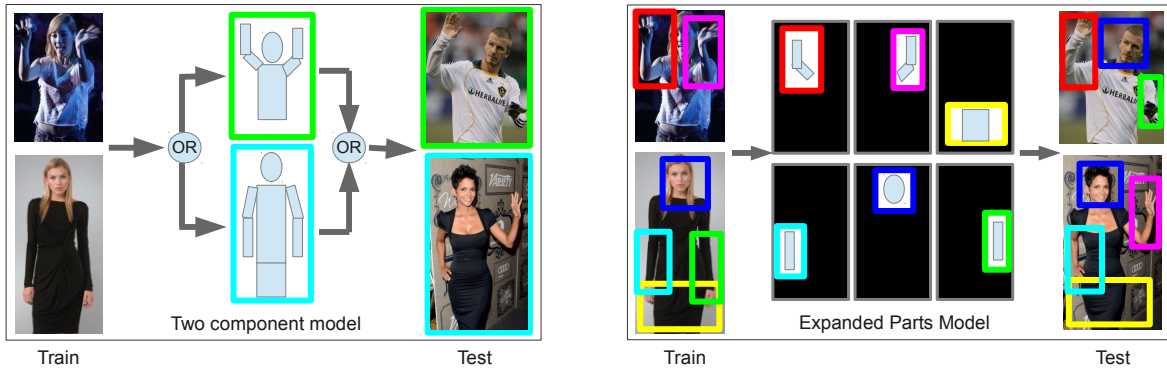


Fig. 2. Illustration of a two-component model vs. the proposed Expanded Parts Model. In a component-based model (left) each training image contributes to the training of a single model and, thus, its parts only score similar images. In contrast, the proposed EPM automatically mines discriminative parts from all images and uses all parts during testing. Also, while for component-based models, only images with typical training variations can be scored reliably, in the proposed EPM sub-articulations can be combined and score untypical variations not seen during training.

obvious what the parts might be and, in particular, should they be the same as, or inspired by, the biologic/anatomic parts. Thus, the proposed method does not make any assumptions on what the parts might be, but instead mines the parts most relevant to the task, and jointly learns their discriminative templates, from among a large set of randomly sampled (in scale and space) candidate parts. Given a test image, EPM recognizes a certain action or attribute by scoring it with the corresponding learnt part templates. As human attributes and actions are often localized in space, e.g. shoulder regions for ‘wearing a tank top’, our model explains the images only partially with the most discriminative regions, as illustrated in Fig. 1 (right). During training we select sufficiently discriminative spatial evidence and do not include regions with low discriminative value or regions containing non-discriminative background. The parts in an EPM compete to explain an image, and different parts might be used for different images. This is in contrast with traditional part based discriminative models where all parts are used for every image.

EPM is inspired by models exploiting sparsity. In their seminal paper, Olshausen and Field [13] argued for a sparse coding with an over-complete basis set, as a possible computation model in the human visual system. Since then sparse coding has been applied to many computer vision tasks, e.g. image encoding for classification [14], [15], image denoising [16], image super-resolution [17], face recognition [18] and optical flow [19]. EPM employs sparsity in two related ways; first the image scoring uses only a small subset of the model parts and second scoring happens with only partially explaining the images spatially. The former model-sparsity is inspired by the coding of information sparsely with an over-complete model, similar to Olshausen and Field’s idea [13]. Owing to such sparsity, while the individual model part interactions are linear, the overall model becomes non-linear [13]. The second spatial sparsity is a result of the simple observation that many of the attributes and actions are spatially localized, e.g. for predicting if a person is wearing a tank top, only the region around the neck and shoulders needs to be inspected, hence the model shouldn’t waste capacity for explaining anything else (in the image space).

To learn an EPM, we propose to use a learning algorithm

based on regularized loss minimization and margin maximization (Sec. 3). The learning algorithm mines important parts for the task, and learns their discriminative templates from a large pool of candidate parts.

Specifically, EPM candidate parts are initialized with  $\mathcal{O}(10^5)$  randomly sampled regions from training images. The learning then proceeds in a stochastic gradient descent framework (Sec. 3.3); randomly sampled training image is scored using up to  $k$  model parts, and the model is updated accordingly (Sec. 3.2). After some passes over the data, the model is pruned by removing the parts which were never used to score any training image sampled so far. The process is repeated for a fixed number of iterations to obtain the final trained EPM. The proposed method is validated on three publicly available datasets of human attributes and actions, obtaining interesting qualitative (Sec. 4.2) and greater than or comparable to state-of-the-art quantitative results (Sec. 4.1). A preliminary version of this work was reported in Sharma et al. [20].

## 2 RELATED WORK

We now discuss the related work on modeling, in particular models without parts, part-based structured models and part-based loosely structured models.

### 2.1 Models without parts

Image classification algorithms have been shown to be successful for the task of human action recognition, see Everingham et al. [7] for an overview of many such methods. Such methods generally learn a discriminative model for each class. For example, in the Spatial Pyramid method (SPM), Lazebnik et al. [21] represent images as a concatenation of bag-of-features (BoF) histograms [22], [23], with pooling at multiple spatial scales over a learnt codebook of local features, like the Scale Invariant Feature Transform (SIFT) of Lowe [24]. Lazebnik et al. [21] then learn a discriminative class model  $\mathbf{w}$  using a margin maximizing classifier, and score an image as  $\mathbf{w}^\top \mathbf{x}$ , with  $\mathbf{x}$  being the image vector. The use of histograms destroys ‘template’ like properties due to the loss of spatial information. Although SPM has never been viewed as a template learning method, methods using gradients based features [25], [26], [27], [28] have

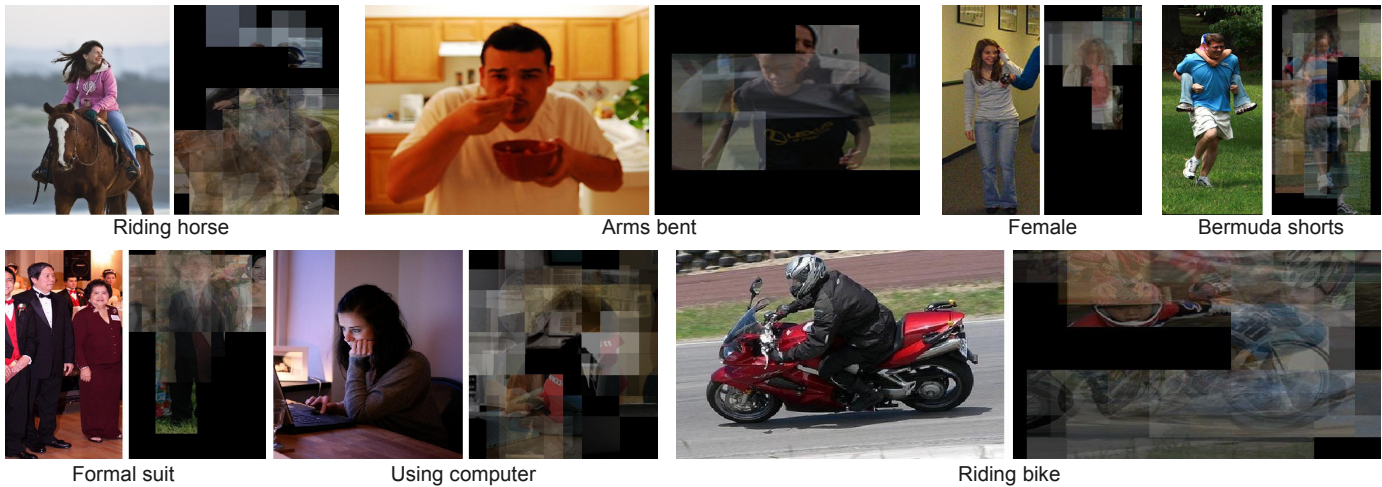


Fig. 3. Illustrations of scoring for different images, for different attributes and actions. Note how the model scores only the discriminative regions in the image while ignoring the non-discriminative or background regions (in black). Such spatial sparsity is particularly interesting when the discriminative information is expected to be localized in space like in the case of many human attributes and actions.

been presented as such, e.g. the recent literature is full of visualizations of templates (class models) learnt with HOG-like [25] features, e.g. [28], [29]. Both, SPM and HOG based, methods have been applied to the task of human analysis [3], [30], where they were found to be successful. We also formulate our model in a discriminative template learning framework. However, we differ in that we learn a collection of templates instead of a single template.

In the recently proposed Exemplar SVM (ESVM) work, Malisiewicz et al. [31] propose to learn discriminative templates for each object instance of the training set independently and then combine their calibrated outputs on test images as a post-processing step. In contrast, we work at a part level and use all templates together during both training and testing. More recently, Yan et al. [32] proposed a 2-level approach for image representation. Similar to our approach it involves sampling image regions, but while they vector quantize the region descriptors, we propose a mechanism to select discriminative regions and build discriminative part based models from them.

Works have also been reported using features which exploit motion for recognizing and localizing human actions in videos [33], [34], [35], [36], [37], [38]. Wang and Schmid [36] use trajectories, Jain et al. use tubelets [34] while Simonyan et al. [38] propose a two-stream convolutional network. Here, we are interested in human action and attribute recognition, but only from still images and hence do not have motion information.

## 2.2 Part-based structured models

Generative or discriminative part-based models (e.g. the Constellation model by Fergus et al. [39] and the Discriminative Part-based Model (DPM) by Felzenszwalb et al. [28]), have led to state-of-the-art results for objects that are rigid or, at least, have a simple and stable structure. In contrast humans involved in actions can have huge appearance variations due to appearance changes (e.g. clothes, hair style, accessories) as well as articulations and poses. Furthermore, their interaction with the context can be very complex. Probably because of the high complexity of tasks

involving humans, DPM does not perform better than SPM for human action recognition as was shown by Delaitre et al. [3]. Increasing the model complexity, e.g. by using a mixture of components [28], has been shown to be beneficial for object detection<sup>1</sup>. Such increase in model complexity is even more apparent in similar models for finer human analysis, e.g. pose estimation [40], [41], [42], where a relatively large number of components and parts are used. Note that components account for coarse global changes in aspect/viewpoint, e.g. full body frontal image, full-body profile image, upper body frontal image and so on, whereas parts account for the local variations of the articulations, e.g. hands up or down. Supported by a systematic empirical study, Zhu et al. [43] recently recommended the design of carefully regularized richer (with a larger number of parts and components) models. Here, we propose a richer and higher capacity model, but less structured, the Expanded Parts Model.

In mixture of components models, the training images are usually assigned to a single component (see Fig. 2 for an illustration) and thus contribute to training one of the templates only. Such clustering like property limits their capability to generate novel articulations, as sub-articulation in different components cannot be combined. Such clustering and averaging are a form of regularization and involve manually setting the number of parts and components. In comparison, the proposed EPM does not enforce similar averaging, nor does it forbid it by definition. It can have a large number of parts (up to the order of the number of training images) if found necessary despite sufficient regularization. Part-based deformable models initialize the parts either with heuristics (e.g. regions with high average energy [28]) or use annotations [40], while EPM systematically explores parts at a large number of locations, scales and atomicities and selects the ones best suited for the task.

<sup>1</sup>. See the results of different versions of the DPM software <http://people.cs.uchicago.edu/~rgb/latent/> which, along with other improvements, steadily increase the number of components and parts.

### 2.3 Part-based loosely structured models

EPM bears some similarity with Poselets by Bourdev et al. [44], [45], [46], [47], which are compound parts consisting of multiple anatomical parts, highly clustered in 3D configuration space, e.g. head and shoulders together. Poselets vote independently for a hypothesis, and are shown to improve performance. However, they are trained separately from images annotated specifically in 3D. In contrast, EPM tries to mine out such parts, at the required atomicity, from given training images for a particular task. Fig. 6 (top right) shows some of the parts for the ‘female’ class which show some resemblance with poselets, though are not as clean.

Methods such as Poselets and the proposed method are also conceptually comparable to the mid-level features based algorithms [48], [49], [50], [51], [52], [53], [54], [55], [56]. While Singh et al. [55] proposed to discover and exploit mid-level features in a supervised or semi-supervised way, with alternating between clustering and training discriminative classifiers for the clusters, Juneja et al. [51] proposed to learn distinctive and recurring image patches which are discriminative for classifying scene images using a seeding, expansion and selection based strategy. Lim et al. [52] proposed to learn small sketch elements for contour and object analysis. Oquab et al. [53] used the mid-level features learnt using CNNs to transfer information to new datasets. Boureau et al. [48] viewed combinations of popular coding and pooling methods as extracting mid-level features and analysed them. Sabzmejdani et al. [54] proposed to learn mid level shapelets features for pedestrian detection. Yao et al. [57] proposed to recognize human actions using bases of human attributes and parts, which can be seen as a kind of mid-level features. The proposed EPM explores the space of such mid-level features systematically under a discriminative framework and more distinctively uses only a subset of model parts for scoring cf. all model parts by the traditional methods. In a recent approach, Parizi et al. [58] propose to mine out parts using a  $\ell_1/\ell_2$  regularization with weights on parts. They alternate between learning the discriminative classifier on the pooled part response vector, and the weight vector on the parts. However, they differ from EPM as they used pooled response of all parts for an image while EPM considers absolute responses of the best subset of parts from among the collection of an over complete set of model parts.

Many methods have also been proposed to reconstruct images using patches, e.g. Similarity by Composition by Boiman and Irani [59], Implicit Shape Models by Leibe et al. [60], Naive Bayes Nearest Neighbors (NBNN) by Boiman et al. [61], and Collaborative Representation by Zhu et al. [62]. Similarly sparse representation has been also used for action recognition in videos [63]. However, while such approaches are generative and are generally based on minimizing the reconstruction error, EPM aims to mine out good patches and learn corresponding discriminative templates with the direct aim of achieving good classification.

### 2.4 Description of humans other than actions and attributes

Other forms of descriptions of humans have also been reported in the literature. E.g. pose estimation [64], [65], [66],

[67], [68], [69] and using pose related methods for action [70], [71], [72], [73], [74] and attribute [72] recognition have been studied in computer vision. Recognizing attributes from the faces of humans [44], [75], [76], recognizing facial expressions [36], [77], [78], [79] and estimating age from face images [80], [81], [82], [83], [84] have also attracted fair attention. Shao et al. [85] aimed to predict the occupation of humans from images, which can be seen as a high-level attribute. In the present work, we work with full human bodies where the faces may or may not be visible and the range of poses may be unconstrained. Although some of the attributes and actions we consider here are correlated with pose, we do not attempt to solve the challenging problem of pose first and then infer the said attributes and actions. We directly model such actions and attributes from the full appearance of the human, expecting the model to make such latent factorization, implicitly within itself, if required.

In addition to the works mention above, we also refer the reader to Guo and Lai [86], for a survey of the general literature for the task of human action recognition from still images.

## 3 EXPANDED PARTS MODEL APPROACH

We address the problem in a supervised classification setting. We assume that a training set of images and their corresponding binary class labels, i.e.

$$\mathcal{T} = \{(\mathbf{x}_i, y_i) | \mathbf{x}_i \in \mathcal{I}, y_i \in \{-1, +1\}, i = 1, \dots, m\} \quad (1)$$

are available, where  $\mathcal{I}$  is the space of images. We intend to learn a scoring function parametrized by the model parameters  $\Theta$ ,

$$s_\Theta : \mathcal{I} \rightarrow \mathbb{R}, \quad \Theta \in \mathcal{M}, \quad (2)$$

where  $\mathcal{M}$  is a class of models (details below), which takes an image and assigns a real valued score to reflect the membership of the image to the class. In the following we abuse notation and use  $\Theta$  to denote either the parameters of, or the learnt model itself. We define an Expanded Parts Model (EPM) to be a collection of discriminative templates, each with an associated scale space location. Images scoring, with EPM, is defined as aggregating the scores of the most discriminative image regions corresponding to a subset of model parts. The scoring thus (i) uses a specific subset (different for different images) of model parts and (ii) only scores the discriminative regions, instead of the whole image. We make these notions formal in the next section (Sec. 3.1).

### 3.1 Formulation as regularized loss minimization

Our model is defined as a collection of discriminative templates with associated locations, i.e.

$$\Theta \in \mathcal{M} = \{(\mathbf{w}, \ell) | \mathbf{w} \in \mathbb{R}^{Nd}, \ell \in [0, 1]^{4N}\} \quad (3)$$

where  $N \in \mathbb{N}$  is the number of parts,  $d \in \mathbb{N}$  is the dimension of the appearance descriptor,

$$\mathbf{w} = [\mathbf{w}_1, \dots, \mathbf{w}_N], \quad \mathbf{w}_p \in \mathbb{R}^d, \quad p = 1, \dots, N \quad (4)$$

is the concatenation of  $p = 1, \dots, N$  part templates and

$$\ell = [\ell_1, \dots, \ell_N] \in [0, 1]^{4N} \quad (5)$$

is the concatenation of their scale-space positions, with each  $\ell_p$  specifying a bounding box, i.e.

$$\ell_p = [\tilde{x}_1, \tilde{y}_1, \tilde{x}_2, \tilde{y}_2] \in [0, 1]^4, \quad p = 1, \dots, N \quad (6)$$

where  $\tilde{x}$  and  $\tilde{y}$  are fractional multiples of width and height respectively.

We propose to learn our model with regularized loss minimization, over the training set  $\mathcal{T}$ , with the objective

$$L(\Theta; \mathcal{T}) = \frac{\lambda}{2} \|\mathbf{w}\|_2^2 + \frac{1}{m} \sum_{i=1}^m \max(0, 1 - y_i s_\Theta(\mathbf{x}_i)), \quad (7)$$

with  $s_\Theta(\cdot)$  being the scoring function (Sec. 3.2). Our objective is the same as that of linear support vector machines (SVMs) with hinge loss. The only difference is that we have replaced the linear score function, i.e.

$$\tilde{s}_w(\mathbf{x}) = \mathbf{w}^\top \mathbf{x}, \quad (8)$$

with our scoring function. The free parameter  $\lambda \in \mathbb{R}$  sets the trade-off between model regularization and the loss minimization as in the traditional SVM algorithm.

### 3.2 Scoring function

We define the scoring function as

$$s_\Theta(\mathbf{x}) = \max_{\alpha} \frac{1}{\|\alpha\|_0} \sum_{p=1}^N \alpha_p \mathbf{w}_p^\top f(\mathbf{x}, \ell_p) \quad (9a)$$

$$\text{s.t.} \quad \|\alpha\|_0 = k \quad (9b)$$

$$O_v(\alpha, \ell) \leq \beta, \quad (9c)$$

where,  $\mathbf{w}_p \in \mathbb{R}^d$  is the template of part  $p$  and  $f(\mathbf{x}, \ell_p)$  is the feature extraction function which calculates the appearance descriptor of the image  $\mathbf{x}$ , for the patch specified by  $\ell_p$ ,

$$\alpha = [\alpha_1, \dots, \alpha_N] \in \{0, 1\}^N \quad (10)$$

are the binary coefficients which specify if a model part is used to score the image or not,  $O_v(\alpha, \ell)$  measures the extent of overlap between the parts selected to score the image. The  $\ell_0$  norm constraint on  $\alpha$  enforces the use of  $k$  parts for scoring while the second constraint encourages coverage in reconstruction by limiting high overlaps.  $k \in \mathbb{N}$  and  $\beta \in \mathbb{R}$  are free parameters of the model. Intuitively what the score function does is that it uses each model part  $\mathbf{w}_p$  to score the corresponding region  $\ell_p$  in the image  $\mathbf{x}$  and then selects  $k$  parts to maximize the average score, while constraining the overlap measure between the parts to be less than a fixed threshold  $\beta$ .

Our scoring function is inspired by the methods of (i) image scoring with learnt discriminative templates, e.g. [28], [87] and (ii) those of learnt patch dictionary based image reconstruction [16]. We are motivated by these two principles in the following way. First, by incorporating latent variables, which effectively amount to a choice of the template(s) that is (are) being used for the current image, the full-scoring function can be made nonlinear (piecewise linear, to be more precise) while keeping the interaction with each template as linear. This allows learning of more complex and nonlinear models, especially in an Expectation Maximization (EM) type algorithm, where algorithms to learn linear templates can be used once the latent variables

are fixed, e.g. [28], [87]. Second, similar to the learnt patch dictionary-based reconstruction, we want to have a spatially distributed representation of the image content, albeit in a discriminative sense, where image regions are treated independently instead of working with a monolithic global model. With a discriminative perspective, we would only like to score promising regions, and use only a subset of model parts, in the images and ignore the background or non-discriminative parts. Exploiting this could be quite beneficial especially as the discriminative information for human actions and attributes is often localized in space, i.e. for ‘riding horse’ only the rider and the horse are discriminative and not the background and for ‘wearing shorts’ only the lower part of the (person centric) image is important. In addition, the model could be over-complete and store information about the same part at different resolutions, which could lead to possible over-counting, i.e. scoring same image region multiple times with different but related model parts, as well; not forcing the use of all model parts can help avoid this over-counting.

Hence, we design the scoring function to score the images with the model parts which are most capable of explaining the possible presence of the class in the image, while (i) using only a subset of relevant parts from the set of all model parts and (ii) penalizing high overlap of parts used, to exploit localization and avoid over-counting as discussed above. We aim, thus, to score the image content only partially (in space) with the most important parts only.

We confirm such behavior of the model with qualitative results in Sec. 4.2.

### 3.3 Solving the optimization problem

We propose to solve the model optimization problem using stochastic gradient descent. We use the stochastic approximation to the sub-gradient w.r.t.  $\mathbf{w}$  given by,

$$\nabla_{\mathbf{w}} L = \lambda \mathbf{w} - \delta_i \frac{1}{\|\alpha\|_0} \begin{bmatrix} \alpha_1 f(\mathbf{x}, \ell_1) \\ \vdots \\ \alpha_N f(\mathbf{x}, \ell_N) \end{bmatrix} \quad (11)$$

where,  $\alpha_p$  are obtained by solving Eq. 9 and

$$\delta_i = \begin{cases} 1 & \text{if } y_i s_\Theta(\mathbf{x}) < 1 \\ 0 & \text{otherwise.} \end{cases} \quad (12)$$

Alg. 1 gives the pseudo-code for our learning algorithm. The algorithm proceeds by scoring (and thus calculating the  $\alpha$  for) the current example with  $\mathbf{w}$  fixed, and then updating  $\mathbf{w}$  with  $\alpha$  fixed, like in a traditional EM like method.

The scoring function is a constrained binary linear program which is NP-hard. Continuous relaxations is a popular way of handling such optimizations, i.e. relax the  $\alpha_i$  to be real in the interval  $[0, 1]$  and replace  $\|\alpha\|_0$  with  $\|\alpha\|_1$ , and then solve the resulting continuous constrained linear program and obtain the binary values by thresholding/rounding the continuous optimum obtained. However, managing the overlap constraint with continuously selected parts would require additional thought. We instead, decide to take a simpler and direct route via an approximate greedy approach. Starting with an empty set of selected parts, we greedily add to it the best scoring part which

**Algorithm 1** SGD for learning Expanded Parts Model (EPM)

---

```

1: Input: Training set  $\mathcal{T} = \{(\mathbf{x}_i, y_i)\}_{i=1}^m$ ; denote  $m^+$  ( $m^-$ )
   as number of positive (negative) examples
2: Returns: Learned Expanded Parts Model,  $\Theta = (\mathbf{w}, \ell)$ 
3: Initialize:  $\Theta = (\mathbf{w}, \ell)$ , rate ( $\eta_0$ ), number of parts for
   scoring ( $k$ ) and regularization constant ( $\lambda$ )
4: for iter = 1, ..., 10 do
5:    $\eta_{+1} \leftarrow \eta_0 \times m^- / m$  and  $\eta_{-1} \leftarrow \eta_0 \times m^+ / m$ 
6:   for npass = 1, ..., 5 do
7:      $\mathcal{S} \leftarrow \text{rand\_shuffle}(\mathcal{T})$ 
8:     for all  $(\mathbf{x}_i, y_i) \in \mathcal{S}$ 
9:       Solve Eq. 9 to get  $s_{\Theta}(\mathbf{x}_i)$  and  $\alpha$ 
10:       $\delta_i \leftarrow \text{binarize}(y_i s_{\Theta}(\mathbf{x}_i) < 1)$ 
11:       $\mathbf{w} \leftarrow \mathbf{w}(1 - \eta_{y_i} \lambda) + \delta_i y_i \eta_{y_i} \sum \alpha_p f(\mathbf{x}_i, \ell_p)$ 
12:    end for
13:  end for
14:  parts_image_map  $\leftarrow \text{note\_image\_parts}(\Theta, \mathcal{S})$ 
15:   $M \leftarrow \text{prune\_parts}(\Theta, \text{parts\_image\_map})$ 
16:  if iter = 5 do  $\eta \leftarrow \eta / 5$  end if
17: end for

```

---

does not overlap appreciably with all the currently selected parts, for the current image. The overlap is measured using intersection over union [7] and two parts are considered to overlap significantly with each other if their intersection over union is more than 1/3. During training we have an additional constraint on scoring, i.e.  $\alpha^\top J \leq \mathbf{1}$ , where  $J \in \{0, 1\}^{N \times m}$  with  $J(p, q) = 1$  if  $p^{\text{th}}$  part was sampled from the  $q^{\text{th}}$  training image, 0 otherwise. The constraint is enforced by ignoring all the parts that were initialized from the training images of the currently selected parts. This increases the diversity of learned parts, by discouraging similar or correlated parts (which emerge from the same training image initially) to score the current image. While training, we score each training image from the rest of the train set, i.e. we do not use the model parts which were generated from the same training image to avoid obvious trivial part selection.

Usually, large databases are highly unbalanced, i.e. they have many more negative examples than positive examples (of the order of 50:1). To handle this we use asymmetric learning rates proportional to the number of examples of other class<sup>2</sup> (Step 4, Alg. 1).

### 3.4 Mining discriminative parts

One of our main intentions is to address important limitations of the current methods: automatically selecting the task-specific discriminative parts at the appropriate scale space locations. The search space for finding such parts is very high, as all possible regions in the training images are potential candidates to be discriminative model parts. We address part mining by two major steps. First, we resort to randomization for generating the initial pool of candidate model parts. We randomly sample part candidates from all the training images, to initialize a highly redundant model. Second, we mine out the discriminative parts from this set by successive pruning. With our learning set in a stochastic

2. [88] achieve the same effect by biased sampling from the two classes.

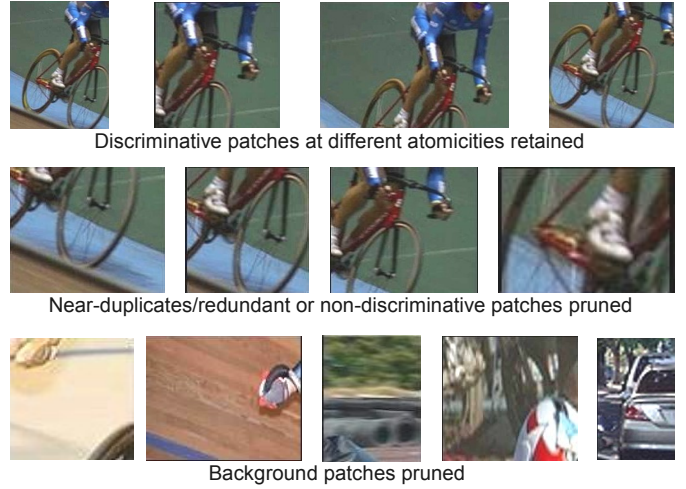


Fig. 4. Example patches illustrating pruning for the ‘riding a bike’ class. While discriminative patches (top) at multiple atomicities are retained by the system, redundant or non-discriminative patches (middle) and random background (bottom) patches are discarded. The patches have been resized and contrast adjusted, for better visualization.

paradigm, we proceed as follows. We first perform a certain number of passes over randomly shuffled training images and keep track of the parts used while updating them to learn the model (recall that not all parts are used to score images and, hence, potentially not all parts in the model, especially when it is highly redundant initially, will be used to score all the training images). We then note that the parts which are not used by any image will only be updated due to the regularization term and will finally get very small weights. We accelerate this shrinking process, and hence the learning process, by pruning them. Such parts are expected to be either redundant or just non-discriminative background; empirically we found that to be the case; Fig. 4 shows some examples of the kind of discriminative parts, at multiple atomicities, that were retained by the model (for ‘riding a bike’ class) while also some redundant parts as well as background parts which were discarded by the algorithm.

### 3.5 Relation with latent SVM

Our Expanded Parts Model learning formulation is similar to a latent support vector machine (LSVM) formulation, which optimizes (assuming a hinge loss function)

$$L(\mathbf{w}; \mathcal{T}) = \frac{\lambda}{2} \|\mathbf{w}\|_2^2 + \frac{1}{m} \sum_{i=1}^m \max(0, 1 - y_i s_L(\mathbf{x}_i)), \quad (13)$$

where the scoring function is given as

$$s_L(\mathbf{x}) = \max_{\mathbf{z}} \mathbf{w}^\top g(\mathbf{x}, \mathbf{z}), \quad (14)$$

with  $\mathbf{z}$  being the latent variable (e.g. part deformations in Deformable Parts-based Model (DPM) [28]) and  $g(\cdot)$ , the feature extraction function. The  $\alpha$ , in our score function Eq. 9, can be seen as the latent variable (one for each image). Consequently, the EPM can be seen as a latent SVM similar to the recently proposed model for object detection by Felzenszwalb et al. [28].

In such latent SVM models the objective function is semi-convex [28], i.e. it is convex for the negative examples. Such semi-convexity follows from the convexity of scoring function, with similar arguments as in Felzenszwalb et al. (Sec. 4 in [28]). The scoring function is a max over functions which are all linear in  $\mathbf{w}$ , and hence is convex in  $\mathbf{w}$  which in turn makes the objective function semi-convex. Optimizing while exploiting semi-convexity gives guarantees that the value of the objective function will either decrease or stay the same with each update. In the present case, we do not follow Felzenszwalb et al. [28] in training, i.e. we do not exploit semi-convexity as in practice we did not observe a significant benefit in doing so. Despite there being no theoretical guarantee of convergence, we observed that, if the learning rate is not aggressive, training as proposed leads to good convergence and performance. Fig. 5 shows a typical case demonstrating the convergence of our algorithm, it gives the value of the objective function, the evolution of the model, in terms of number of parts, and the performance of the system vs. iterations (Step 4, Alg. 1), for ‘interacting with a computer’ class of the Willow Actions dataset.

### 3.6 Appearance features and visualization of scoring

As discussed previously, HOG features are not well adapted to human action recognition. We therefore resort, in our approach, to using appearance features, i.e. the bag-of-features (BoF), for EPM. When we use such appearance representation, the so-obtained discriminative models (similar to [21]) cannot be called templates (cf. HOG based templates [25]). Thus, in the following, we use the word template to loosely denote the similar concept in the appearance descriptor space. Note, however, that the proposed method is feature-agnostic and can be potentially used with any arbitrary appearance descriptor, e.g. BoF [22], [23], HOG [25], GIST [89], CNN [90] etc.

Since we initialize our parts with the appearance descriptors (like BoF) of patches from training images (see Sec. 4 for details), we can use the initial patches to visualize the scoring instead of the final learnt templates as in the HOG case. This is clearly a loose association as the initial patches evolve with training iterations to give the part templates  $\mathbf{w}_p$ . However we hope that the appearance of the initial patch will suffice as a proxy for visualizing the part. We found such an approximate strategy to give reasonable visualizations, e.g. Fig. 3 shows some visualizations of scoring for different classes. While the averaging is not very good, the visualizations do give an approximate indication of which kind of image regions are scored and by which kinds of parts. We discuss these more in the qualitative results Sec. 4.2.

### 3.7 Efficient computation using integral histograms

Since we work with a large number of initial model parts, e.g.  $\mathcal{O}(10^5)$ , the implementation of how such parts are used to score the images becomes an important algorithmic design aspect. In the naïve approach, the scoring will require computing features for  $N$  local regions corresponding to each of the model part. Since  $N$  can be very large for the initial over-complete models, this is intractable. To circumvent this we use integral histograms [91], i.e. 3D data

structure where we keep integral images corresponding to each dimension of the appearance feature. The concept was initially introduced by Crow [92] as summed area tables for texture mapping. It has had a lot of successful applications in computer vision as well [93], [94], [95], [96].

We divide the images with axis aligned regular grid containing rectangular non-overlapping cells. Denote the location of the lattice points of the grid by  $\mathcal{X}^g = \{x_1^g, \dots, x_s^g\}$ ,  $\mathcal{Y}^g = \{y_1^g, \dots, y_t^g\}$ , where,  $x^g, y^g \in [0, 1]$  are fractional multiples of width and height, respectively. We compute the BoF histograms for image regions from  $(0, 0)$  to each of lattice points  $(x_i, y_j)$ , i.e. we compute the feature tensor  $F_{\mathbf{x}} \in \mathbb{R}^{s \times t \times d}$ , for each image  $\mathbf{x}$ , where the  $d$  dimensional vector corresponding to  $F(i, j, \cdot)$  is the corresponding un-normalized BoF vector. When we do random sampling to get candidate parts to initialize the model (details in Sec. 4), we align the parts to the grid, i.e.  $\ell_p = [\tilde{x}_1, \tilde{y}_1, \tilde{x}_2, \tilde{y}_2]$ , s.t.  $\tilde{x}_1 = x_i^g$ ,  $\tilde{y}_1 = y_j^g$ ,  $\tilde{x}_2 = x_k^g$ ,  $\tilde{y}_2 = y_l^g$ ,  $\forall$  some  $i, k \in \{1, \dots, s\}$  and  $j, l \in \{1, \dots, t\}$ .

Hence, to score an image with a part we can efficiently compute the feature for the corresponding location as,

$$f(\mathbf{x}, \ell_p) = F_{\mathbf{x}}(x_k^g, y_l^g, \cdot) + F_{\mathbf{x}}(x_i^g, y_j^g, \cdot) - F_{\mathbf{x}}(x_i^g, y_l^g, \cdot) - F_{\mathbf{x}}(x_k^g, y_j^g, \cdot). \quad (15)$$

$f(\mathbf{x}, \ell_p)$  is then normalized appropriately before computing the score by a dot product with  $\mathbf{w}_p$ . In this way we do not need to compute the features from scratch, for all regions corresponding to the model parts every time an image needs to be scored. Also, this way we need to cache a fixed amount of data, i.e. tensor  $F_{\mathbf{x}}$  for every image  $\mathbf{x}$ .

## 4 EXPERIMENTAL RESULTS

We now present the empirical results of the different experiments we did to validate and analyze the proposed method. We first give the statistics of the datasets then give implementation details of our approach as well as our baseline and, finally, proceed to present and discuss our results on the three datasets.

**The datasets.** We validate and empirically analyze our method on three challenging publicly available datasets:

- 1) *Willow 7 Human Actions*<sup>3</sup> [3] is a challenging dataset for action classification on unconstrained consumer images downloaded from the internet. It has 7 classes of common human actions, e.g. ‘ridingbike’, ‘running’. It has at least 108 images per class of which 70 images are used for training and validation and the rest are used for testing. The task is to predict the action being performed given the human bounding box.
- 2) *27 Human Attributes (HAT)*<sup>4</sup> [4] is a dataset for learning semantic human attributes. It contains 9344 unconstrained human images obtained by applying a human detector [28] on images downloaded from the internet. It has annotations for 27 attributes based on sex, pose (e.g. standing, sitting), age (e.g. young, elderly) and appearance (e.g. wearing a tee-shirt, shorts). The dataset has train, validation and test sets. The models are learnt

3. <http://www.di.ens.fr/willow/research/stillactions/>

4. <http://jurie.users.greyc.fr/datasets/hat.html>

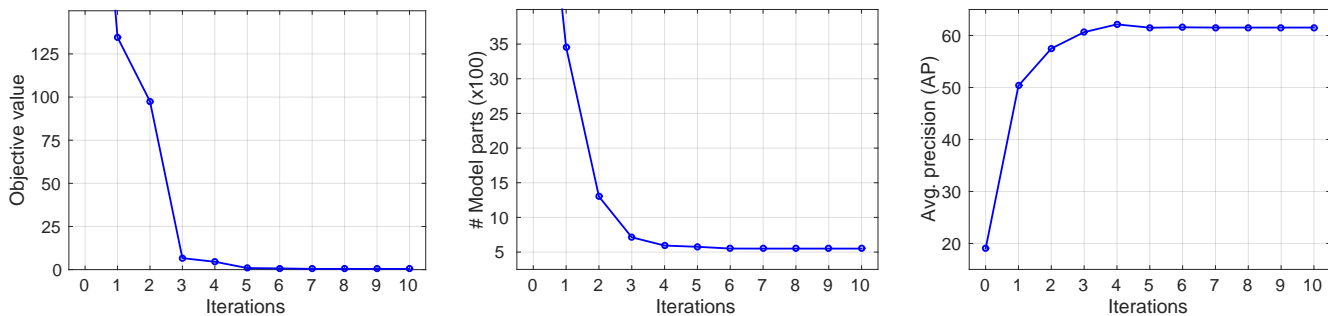


Fig. 5. The evolution of the (left) objective value, (middle) number of model parts along with the (right) average precision vs. number of iterations, for the validation set of ‘interacting with a computer’ class of the Willow Actions dataset, demonstrating the convergence of our algorithm.

with the train and validation sets and the performance is reported on the test set.

- 3) *Stanford 40 Human Actions*<sup>5</sup> [57] is a dataset of human actions with 40 diverse daily human actions, e.g. brushing teeth, cleaning the floor, reading books, throwing a frisbee. It has 180 to 300 images per class with a total of 9352 images. We used the suggested train and test split provided by the authors on the website, with 100 images per class for training and the rest for testing.

All images are human-centered, i.e. the human is assumed to be correctly detected by a previous stage of the pipeline. On all the three datasets, the performance is evaluated with average precision (AP) for each class and the mean average precision (mAP) over all classes.

**BoF features and baseline.** Like previous work [3], [5], [6] we densely sample grayscale SIFT features at multiple scales. We use a fixed step size of 4 pixels and use square patch sizes ranging from 8 to 40 pixels. We learn a vocabulary of size 1000 using k-means and assign the SIFT features to the nearest codebook vector (hard assignment). We use the VLFeat library [97] for SIFT and k-means computation. We use a four-level spatial pyramid with  $\mathcal{C} = \{c \times c | c = 1, 2, 3, 4\}$  cells [21] as a baseline. To have non-linearity we use explicit feature map [98] with the BoF features. We use a map corresponding to the Bhattacharyya kernel, i.e. we take dimension-wise square roots of our  $\ell_1$  normalized BoF histograms obtaining  $\ell_2$  normalized vectors, which we use with the baseline as well as with our algorithm. The baseline results are obtained with the liblinear [99] library.

**Context.** The immediate context around the person, which might contain partially an associated object (e.g. horse in riding horse) and/or correlated background (e.g. grass in running), has been shown to be beneficial for the task [3], [5]. To include immediate context we expand the human bounding boxes by 50% in both width and height. The context from the full image has also been shown to be important [3]. To use it with our method, we add the scores from a classifier trained on full images to scores from our method. The full image classifier uses a 4 level SPM with an exponential  $\chi^2$  kernel.

**Initialization and regularization constant.** In the initialization we intend to generate a large number of part can-

didates, which are subsequently refined by pruning. To achieve this, we randomly sample the positive training images for patch positions, i.e.  $\{\ell_p\}$  and initialize our model parts as

$$\mathbf{w}_p = \begin{bmatrix} 2f(\mathbf{x}, \ell_p) \\ 1 \end{bmatrix}, \quad p = 1, \dots, N \quad (16)$$

where  $\mathbf{x}$  denotes a BoF histogram. Throughout our method, we append 1 at the end of all our BoF features to account for the bias term (cf. SVM, e.g. [88]). This leads to a score of 1 when a perfect match occurs,

$$\mathbf{w}_p^T \begin{bmatrix} f(\mathbf{x}, \ell_p) \\ 1 \end{bmatrix} = [2f(\mathbf{x}, \ell_p), 1] \begin{bmatrix} f(\mathbf{x}, \ell_p) \\ -1 \end{bmatrix} = 1, \quad (17)$$

and a score of  $-1$  in the opposite case, as the appearance features are  $\ell_2$ -normalized. For the learning rate, we follow recent work [88] and fix a learning rate which we reduce once for annealing by a factor of 5 halfway through the iterations (Step 15, Algorithm 1). We follow [88] and fix the regularization constant  $\lambda = 10^{-5}$ .

**Deep CNN features.** Recently, deep Convolutional Neural Networks (CNN) have been very successful, e.g. for image classification [90], [100] and object detection [101], [102], [103], and have been applied for human action recognition in videos [104]. Following such works, we also evaluated the performances of using the recent highly successful deep Convolutional Neural Networks architectures for image classification [90], [100]. Such networks are trained on large external image classification datasets such as the Imagenet dataset [105] and have been shown to be successful with a large variety of computer vision tasks [106]. We used the publicly available `matconvnet` library [107] and the models, pre-trained on the Imagenet dataset, corresponding to the network architectures proposed by Krizhevsky et al. [90] (denoted AlexNet) and by Simonyan and Zisserman [100] (16 layer network; denoted VGG-16).

#### 4.1 Quantitative results

Tab. 1 shows the results of the proposed Expanded Parts Model (EPM) (with and without context) along with our implementation of the baseline Spatial Pyramid [21] (SPM) and some competing methods using similar features, on the Willow 7 Actions dataset. We achieve a mAP of 66% which goes up to 67.6% by adding the full image context. We perform better than the current state-of-the-art method

5. <http://vision.stanford.edu/Datasets/40actions.html>

TABLE 1  
Performances (mAP) on the Willow Actions dataset

Class	[28]	[8]	[5]	[21]	EPM	EPM+C
intr. w/ comp.	30.2	56.6	59.7	59.7	60.8	64.5
photographing	28.1	37.5	42.6	42.7	40.5	40.9
playing music	56.3	72.0	74.6	69.8	71.6	75.0
riding bike	68.7	90.4	87.8	89.8	90.7	91.0
riding horse	60.1	75.0	84.2	83.3	87.8	87.6
running	52.0	59.7	56.1	47.0	54.2	55.0
walking	56.0	57.6	56.5	53.3	56.2	59.2
mean	50.2	64.1	65.9	63.7	66.0	67.6

[5] (with similar features) on this dataset on five out of seven classes and on average. As demonstrated by [3], full image context plays an important role in this dataset. It is interesting to note that even without context, we achieve 3.5% absolute improvement compared to a method which models person-object interactions [8] and uses extra data to train detectors.

The second last column in Tab. 2 (upper part) shows our results, with bag-of-features based representations, along with results of the baseline SPM and other methods, on the Stanford 40 Actions. EPM performs better than the baseline by 5.8% (absolute) at 40.7%. It also performs better than Object bank [108] and Locality-constrained linear coding [109] (as reported in [57]) by 8.2% and 5.5% respectively. With context, EPM achieves 42.2% mAP which is the state-of-the-art result using no external training data and grayscale features only. Yao et al. [57] reported higher performance on this dataset (45.7%), by performing action recognition using bases of attributes, objects and poses. To derive their bases they use pre-trained systems for 81 objects, 45 attributes and 150 poselets, using large amount (comparable to the size of the dataset) of external data. Since they use human based attributes also, arguably, EPM can be used to improve their generic classifiers and improve performance further, i.e. EPM is complementary to theirs. Khan et al. [30] also report higher (51.9%) performance on the dataset fusing multiple features, particularly those based on color, while here we have used only grayscale information.

The last column in Tab. 2 (upper part) shows ours as well as other results, with bag-of-features based representations, on the dataset of Human Attributes. Our baseline SPM is already higher than the results reported by the dataset creators [4], because we use denser SIFT and more scales. EPM improves over the baseline by 3.2% (absolute) and increases further by 1% when adding the full image context. EPM (alone, without context) outperforms the baseline for 24 out of the 27 attributes. Among the different human attributes, those based on pose (e.g. standing, arms bent, running/walking) are found to be easier than those based on appearance of clothes (e.g. short skirt, bermuda shorts). The range of performance obtained with EPM is quite wide, from 24% for crouching to 98% for standing.

Tab. 2 (bottom part) shows the results of the CNN features, on the person bounding box and the whole image, as well as their combinations with EPM (averaging of the scores of combined methods), on the two larger datasets, i.e. Stanford 40 Actions and Human Attributes. We can make the following interesting observations from Tab. 2

TABLE 2  
Performances (mAP) of EPM and deep Convolutional Neural Networks on the Stanford 40 Actions and the Human Attributes datasets

Method	Image region	Stan40	HAT
Discr. Spatial Repr. [4]	bounding box	-	53.8
Appearance dict. [50]		-	59.3
SPM (baseline) [21]		34.9	55.5
Object bank [108]	full image	32.5	-
LLC coding [109]	bb + full img	35.2	-
EPM	bounding box	40.7	58.7
EPM + Context	bb + full img	42.2	59.7
AlexNet (B) [90]	bounding box	44.0	60.7
VGG-16 (B) [100]		61.3	64.8
AlexNet (I)	full image	56.8	51.7
VGG-16 (I)		70.6	55.4
EPM + AlexNet (B)	bounding box	50.7	66.0
EPM + VGG-16 (B)		64.0	<b>69.6</b>
EPM + AlexNet (I)	bb + full img	60.2	62.2
EPM + VGG-16 (I)		<b>72.3</b>	64.2

(bottom part). First, the performance of the deep features computed on bounding boxes vs. the one on full images follows inverse trends on the two datasets. On the Stanford Actions dataset, (i) the images are relatively cleaner (ii) mostly have one prominent person per image and (iii) many classes are scene dependent, e.g. ‘fixing a bike’, ‘feeding a horse’ – as a result the deep features on the full image perform better than those on the person bounding boxes. On the other hand, the Human Attributes dataset often has multiple people per image with more scale variations and the classes are person focused, e.g. ‘wearing a suit’, ‘elderly’, thus, the deep features on the person bounding boxes are better than those on the full images. Second, we see that the proposed Expanded Parts Model (EPM) based classifier is not very far in performance from AlexNet (3.3% and 2% absolute for the two datasets). This is quite encouraging as the deep features are trained on large amount of external data and use the color information of the images, while the EPM is only trained on the respective training data of the datasets and uses grayscale information only. The stronger VGG-16 network is much better than both EPM and AlexNet. It is quite interesting to note that EPM is strongly complementary to the deep features. When using deep features on person bounding boxes, it improves performance by 6.7% and 2.7% on Stanford Actions and by 5.3% and 4.8% on Human Attributes, of AlexNet and VGG-16 networks respectively. When using deep features on full images, the improvements are 3.4% and 1.7% for Stanford Actions and 10.5% and 8.8% for Human Attributes datasets.

As deep features are not additive like bag-of-features histograms (feature for two image regions together is not the sum of features for each separately) we can’t use the integral histograms based efficient implementation with the deep features and computing and caching features for all candidate parts is prohibitive. Hence, we can’t use the deep features out-of-the-box with our method. Tailoring EPM for use with deep architectures is an interesting extension but is out of scope of the present work.

## 4.2 Qualitative results

We present qualitative results to illustrate the scoring, Fig. 3 shows some examples, i.e. composite images created by

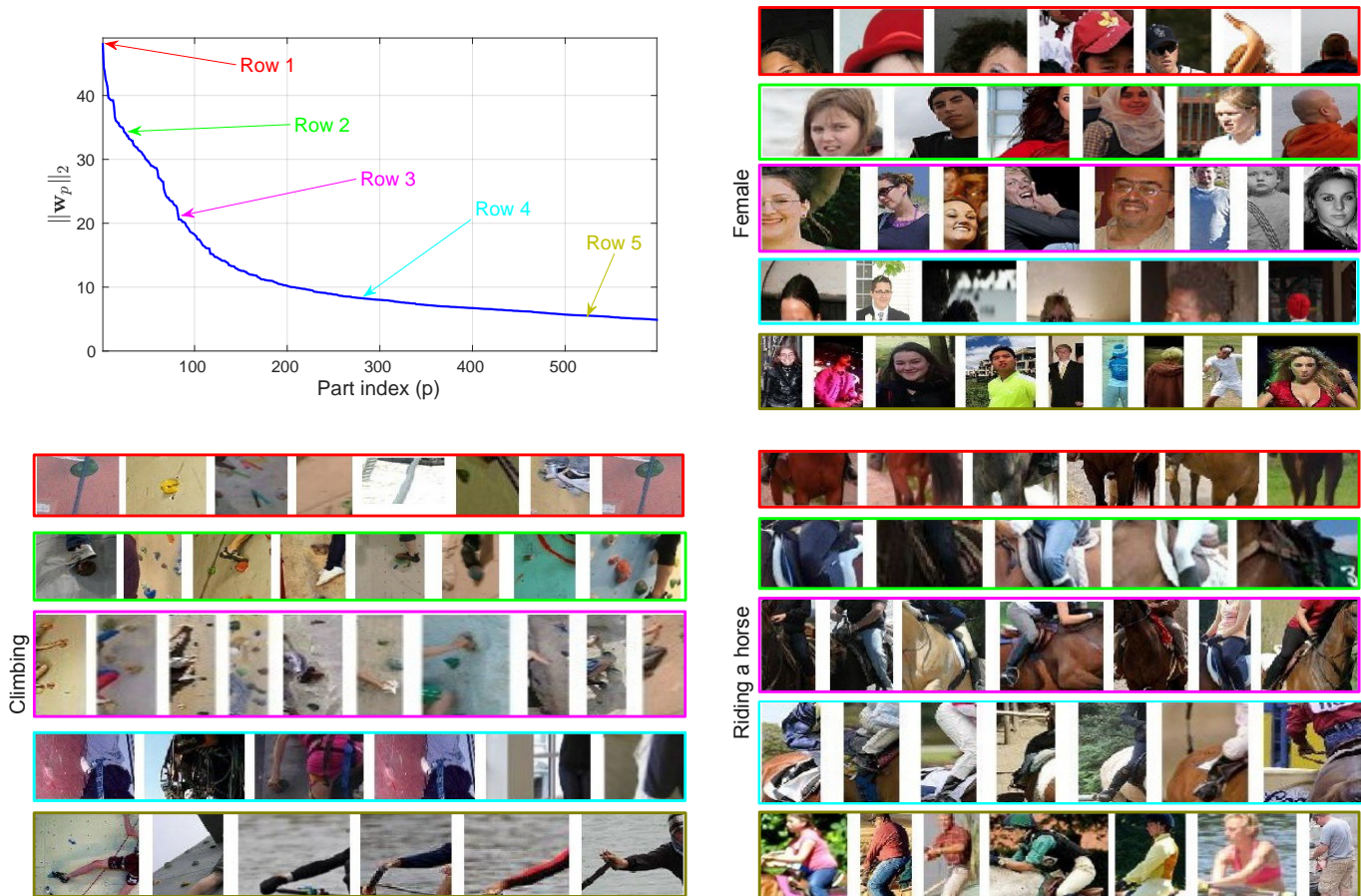


Fig. 6. Distribution of the norm of the part templates (left top) and some example ‘parts’ (rest three). Each row illustrates one of the parts: the first image is the patch used to initialize the part and the remaining images are its top scoring patches. We show, for each class, parts with different norms (color coded) of the corresponding  $w_p$  vectors, higher (lower) norm part at top (bottom). (see Sec. 4.3 for a discussion, best viewed in color).

averaging the part patches with non-zero alphas. We can observe that the method focuses on the relevant parts, such as torso and arms for ‘bent arms’, shorts and tee-shirts for ‘wearing bermuda shorts’, and even computer (left bottom) for ‘using computer’. Interestingly, we observe that for both ‘riding horse’ and ‘riding bike’ classes, the person gets ignored but the hair and helmet have been used partially for scoring. We explain this with the discriminative nature of the learnt models: as people in similar pose might confuse the two classes, the models ignore it and focus on other more discriminative aspects.

### 4.3 The parts mined by the model

Fig. 6 shows the distribution of the  $\ell_2$  norm of the learnt part templates, along with top scoring patches for the selected parts, with norms across the spectrum for three classes. The first image in any row is the patch with which the part was initialized and the remaining ones are its top scoring patches. The top scoring patches give an idea of what kind of appearances the learnt templates  $w_p$  capture. We observe that, across datasets, while most of the parts seem interpretable, e.g. face, head, arms, horse saddle, legs, there are a few parts that seem to correspond to random background (e.g. row 1 for ‘climbing’). This is in line with a recent study [43], in ‘mixture of template’ like formulations,

there are clean interpretable templates along with noisy templates which correspond to background.

We also observe that the distribution of the  $\ell_2$  norm of the parts follows a heavy tailed distribution. Some parts are very frequent and the system tries to tune them to give high scores for positive vectors and low scores for negative vectors and hence give them a high overall energy. There are also parts which have smaller norms, either because they are consistent in appearance (like the head and partial shoulders on clean backgrounds in row 4 of ‘female’ Fig. 6, or the leg/arm in the last row of ‘climbing’) or occur in few images. However, they are discriminative nonetheless.

Fig. 8 (left and middle) shows the relation between the performances and the number of model parts, for the different classes of the larger Stanford Actions and Human Attributes datasets. The right plot gives the number of training images vs. the number of model parts for the different classes of the Human Attributes dataset (such curve is not plotted for the Stanford Actions dataset as it has the same number of training images for each class). We observe that the model sizes and the performances for the classes are correlated. On the Stanford Actions dataset, which has the same number of training images for every class, on an average, class models with a higher number of parts obtain higher performance (correlation coefficient between number of parts and performances of 0.47). This

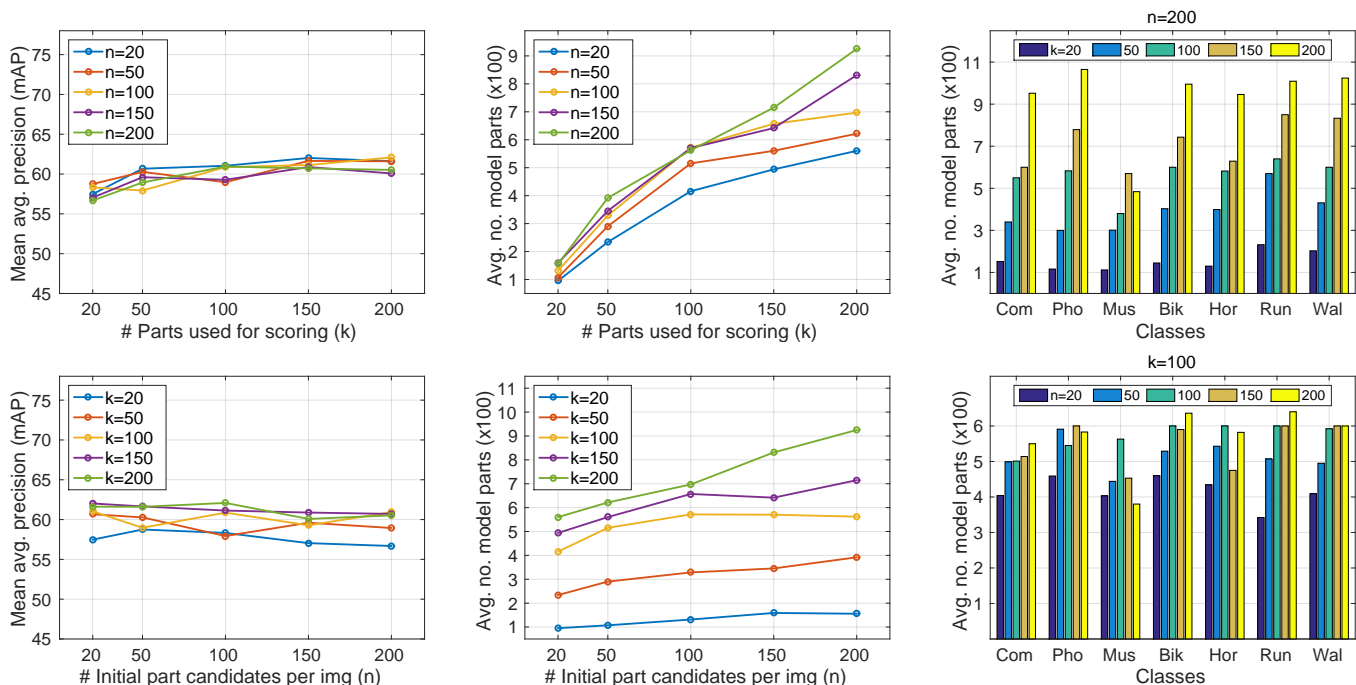


Fig. 7. Experiments to evaluate the impact of the number of parts and the number of initial candidate parts on the performance of the proposed model on the validation set of the Willow Actions dataset (see Tab. 1 for the full class names). The first row shows the performances and number of model parts for different values of  $k$ , i.e. the maximum number of model parts used to score a test image, while the second row shows those for varying  $n$ , i.e. the number of initial part candidates sampled per training image.

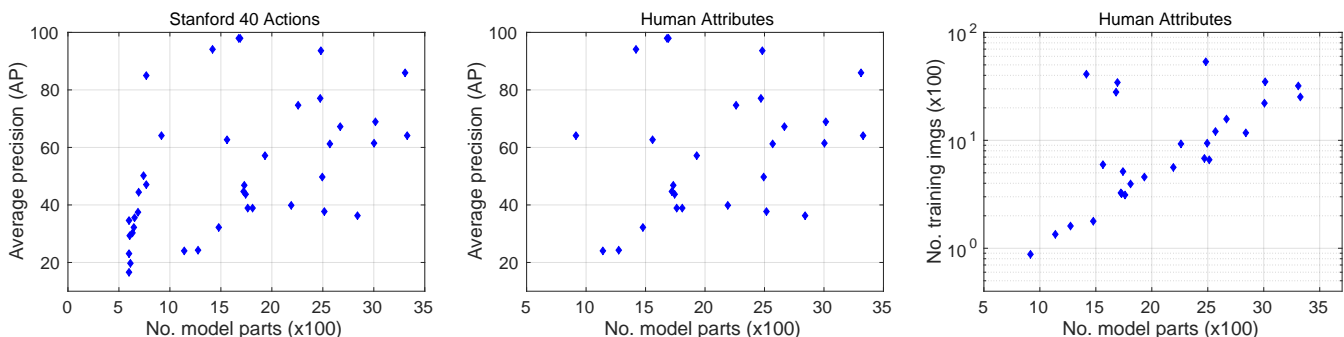


Fig. 8. The average precision obtained by the models for (left) Stanford Actions, (middle) HAT dataset and (right) the number of training images (for HAT; the number of training images for Stanford Actions dataset is same for all classes) vs. the number of parts in the final trained models of the different classes (see Sec. 4.3 for discussion).

is somewhat counter intuitive as we would expect that the model with larger number of parts, and hence larger number of parameters/higher capacity, would over-fit cf. those with smaller number of parts, for the same amount of training data for both cases. However, this can be explained as follows. The classes where there are large amounts of variations which are well captured by the train set, the model admits larger number of parts to explain the variations and then successfully generalizes to the test set. While for classes where the train set captures only a limited amount of variation, the model fits on the train set with a smaller number of parts but is then unable to generalize well to the test set with different variations. An intuitive feeling of such variations can be had by noting the classes which are relatively well predicted, e.g. ‘climbing’, ‘riding a horse’, ‘holding an umbrella’, vs. those that are not so well predicted, e.g. ‘texting message’, ‘waving hands’, ‘drinking’

– while the former classes are expected to have more visual coherence, the latter are expected to be relatively more visually varied.

Similar correlation of the number of model parts with performances (Fig. 8 middle) is also observed for Human Attributes dataset (albeit weaker with correlation coefficient 0.23). Since Human Attributes dataset has different number of images for different classes, it allows us to make the following interesting observation as well. The performances for Human Attributes dataset are highly correlated with the number of training images (correlation coefficient 0.79), which is explained simply as the classes with higher number of images have higher chance performance, and the classifiers are accordingly better in absolute performance. However, the relationship between the number of training images and the model parts is close to exponential (correlation coefficient between the log of number of training

images and the number of model parts 0.65). This is interesting as it is in line with the heavy tailed nature of visual information – as the number of images increase the model expands to capture the visual variability quickly initially but as the training data increases further the model only expands when it encounters rarer visual information and hence the growth decreases. The three clear outliers where the increase in training images does not lead to an increase in model size (after a limit) are ‘upperbody’, ‘standing’, ‘arms bent’ — these classes are also the best-performing classes; they have relatively high number of training images but still do not need many model parts as they are limited in their (discriminative) visual variations.

#### 4.4 Effect of parameters

There are two important parameters in the proposed algorithm, first, the number of parts used to score the images  $k$  and, second, the number of candidate parts to be sampled for initializing the model  $n$  (per training image). To investigate the behavior of the method w.r.t. these two parameters, we did experiments on the validation set of the Willow Actions dataset. Fig. 7 shows the performances and the model sizes (number of parts in the final models) when varying these two parameters in the range  $\{20, 50, 100, 150, 200\}$ . We observe that the average number of model parts increases rapidly as  $k$  is increased (Fig. 7 middle-top). This is expected to a certain extent, as the pruning of the model parts is dependent on  $k$ ; if  $k$  is large then a larger number of parts are used per image while training, and hence more parts will be used, on an average, and consequently survive pruning. However, the increase in the model size is not accompanied by a similarly aggressive increase in the validation performance (Fig. 7 left-top). The average number of model parts for  $k = 100$  and  $n = 200$  is 549. Similar increase in the model size but with increase in  $n$  is more varied for different values of  $k$ ; for lower value of say  $k = 20$  the increase in model size with  $n$  is subtle when compared to the same for a higher value of say  $k = 200$ . However, again such increase in model size doesn’t bring increase in validation performance either. It is also interesting to note the behavior of the models of different classes when varying  $k$  and  $n$ . The bar graphs on the right of Fig. 7 show the number of model parts when  $n$  is fixed to 200 and  $k$  is varied (top) and when  $k$  is fixed to 100 and  $n$  is varied. In general, as  $k$  was increased the models of almost all the classes grew in number of parts with  $n$  fixed, while when  $k$  was fixed and more model parts were made available, the models first grew and then saturated. The only exception to this was the ‘playing music’ class where the models practically saturated in both cases, perhaps because of limited appearance variations. The growing of models with increasing  $k$  was followed by a slight drop in the performance, probably due to over-fitting.

Following these experiments and also for keeping a reasonable computational complexity,  $k$  was fixed to  $k = 100$  for the experiments reported. This is also comparable to the 85 cells in the four-level spatial pyramid representation used as a baseline. Similarly,  $n$  was fixed to be  $n = 200$  for the Willow Actions dataset and  $n = 20$  for the about  $10\times$  larger Stanford Action and Human Attributes datasets (recall that

$n$  is the number of initial candidates parts sampled per training image) in the experiments reported.

#### 4.5 Training/testing times

The training is significantly slower compared to a standard SPM/SVM baseline, i.e. by around two orders of magnitude. This is due to the fact that there is SVM equivalent cost (with a larger number of vectors) at each iteration. Testing is also a bit slower compared to an SPM, as it is based on a dot product between longer vectors. For example, on Stanford dataset testing is 5 times slower compared to SPM at about 35 milliseconds per image (excluding feature extraction).

## 5 CONCLUSION

We have presented a new Expanded Parts Model (EPM) for human analysis. The model learns a collection of discriminative templates which can appear at specific scale-space positions. It scores a new image by sparsely explaining only the discriminative regions in the images while using only a subset of the model parts. We proposed a stochastic sub-gradient based learning method which is efficient and scalable – in the largest of our experiments we mine models of  $\mathcal{O}(10^3)$  parts from among initial candidate sets of  $\mathcal{O}(10^5)$ . We validated our method on three challenging publicly available datasets for human attributes and actions. We also showed complementary nature of the proposed method to the current state-of-the-art deep Convolutional Neural Networks based features. Apart from obtaining good quantitative results, we analysed the nature of the parts obtained and also analysed the growth of the model size with the complexity of the visual task as well as the amount of training data available.

## ACKNOWLEDGEMENTS

This work was partly realized as part of the Quaero Programme, funded by OSEO, French State agency for innovation, by the ANR (grant reference ANR-2010-CORD-103-06) and by the ERC advanced grant ALLEGRO.

## REFERENCES

- [1] W. Yang, Y. Wang, and G. Mori, “Recognizing human actions from still images with latent poses,” in *CVPR*, 2010.
- [2] B. Yao and L. Fei-Fei, “Modeling mutual context of object and human pose in human-object interaction activities,” in *CVPR*, 2010.
- [3] V. Delaitre, I. Laptev, and J. Sivic, “Recognizing human actions in still images: A study of bag-of-features and part-based representations,” in *BMVC*, 2010.
- [4] G. Sharma and F. Jurie, “Learning discriminative representation for image classification,” in *BMVC*, 2011.
- [5] G. Sharma, F. Jurie, and C. Schmid, “Discriminative spatial saliency for image classification,” in *CVPR*, 2012.
- [6] B. Yao, A. Khosla, and L. Fei-Fei, “Combining randomization and discrimination for fine-grained image categorization,” in *CVPR*, 2011.
- [7] M. Everingham, L. Van Gool, C. K. I. Williams, J. Winn, and A. Zisserman, “The PASCAL Visual Object Classes Challenge 2011 (VOC2011) Results,” <http://www.pascal-network.org/challenges/VOC/voc2011/workshop/index.html>, 2011.
- [8] V. Delaitre, J. Sivic, and I. Laptev, “Learning person-object interactions for action recognition in still images,” in *NIPS*, 2011.

- [9] C. Desai, D. Ramanan, and C. Fowlkes, "Discriminative models for static human-object interactions," in *CVPR Workshops*, 2010.
- [10] A. Gupta, A. Kembhavi, and L. S. Davis, "Observing human-object interactions: Using spatial and functional compatibility for recognition," *PAMI*, vol. 31, pp. 1775–1789, October 2009.
- [11] A. Prest, C. Schmid, and V. Ferrari, "Weakly supervised learning of interactions between humans and objects," *PAMI*, vol. 34, no. 3, pp. 601–614, 2011.
- [12] B. Yao and L. Fei-Fei, "Grouplet: A structured image representation for recognizing human and object interactions," in *CVPR*, 2010.
- [13] B. A. Olshausen and D. J. Field, "Sparse coding with an over-complete basis set: A strategy employed by v1?" *Vision research*, vol. 37, no. 23, pp. 3311–3325, 1997.
- [14] J. Yang, K. Yu, Y. Gong, and T. Huang, "Linear spatial pyramid matching using sparse coding for image classification," in *CVPR*, 2009.
- [15] J. Yang, K. Yu, and T. Huang, "Efficient highly over-complete sparse coding using a mixture model," in *ECCV*, 2010.
- [16] J. Mairal, F. Bach, J. Ponce, and G. Sapiro, "Online learning for matrix factorization and sparse coding," *JMLR*, vol. 11, pp. 19–60, 2010.
- [17] J. Yang, J. Wright, T. S. Huang, and Y. Ma, "Image super-resolution via sparse representation," *TIP*, vol. 19, no. 11, pp. 2861–2873, 2010.
- [18] J. Wright, A. Y. Yang, A. Ganesh, S. S. Sastry, and Y. Ma, "Robust face recognition via sparse representation," *PAMI*, vol. 31, no. 2, pp. 210–227, 2009.
- [19] K. Jia, X. Wang, and X. Tang, "Optical flow estimation using learned sparse model," in *ICCV*, 2011.
- [20] G. Sharma, F. Jurie, and C. Schmid, "Expanded parts model for human attribute and action recognition in still images," in *CVPR*, 2013.
- [21] S. Lazebnik, C. Schmid, and J. Ponce, "Beyond bags of features: Spatial pyramid matching for recognizing natural scene categories," in *CVPR*, 2006.
- [22] G. Csurka, C. R. Dance, L. Fan, J. Willamowski, and C. Bray, "Visual categorization with bags of keypoints," in *Intl. Workshop on Stat. Learning in Comp. Vision*, 2004.
- [23] J. Sivic and A. Zisserman, "Video Google: A text retrieval approach to object matching in videos," in *ICCV*, 2003.
- [24] D. Lowe, "Distinctive image features form scale-invariant keypoints," *IJCV*, vol. 60, no. 2, pp. 91–110, 2004.
- [25] N. Dalal and B. Triggs, "Histograms of oriented gradients for human detection," in *CVPR*, 2005.
- [26] R. Benenson, M. Mathias, R. Timofte, and L. Van Gool, "Pedestrian detection at 100 frames per second," in *CVPR*, 2012.
- [27] P. Dollár, R. Appel, S. Belongie, and P. Perona, "Fast feature pyramids for object detection," *PAMI*, vol. 36, no. 8, pp. 1532–1545, 2014.
- [28] P. Felzenszwalb, R. Girshick, D. McAllester, and D. Ramanan, "Object detection with discriminatively trained part based models," *PAMI*, vol. 32, no. 9, pp. 1627–1645, 2010.
- [29] M. Pandey and S. Lazebnik, "Scene recognition and weakly supervised object localization with deformable part-based models," in *ICCV*, 2011.
- [30] F. S. Khan, R. M. Anwer, J. van de Weijer, A. D. Bagdanov, A. M. Lopez, and M. Felsberg, "Coloring action recognition in still images," *IJCV*, vol. 105, no. 3, pp. 205–221, 2013.
- [31] T. Malisiewicz, A. Gupta, and A. Efros, "Ensemble of Exemplar-SVMs for object detection and beyond," in *ICCV*, 2011.
- [32] S. Yan, X. Xu, D. Xu, S. Lin, and X. Li, "Beyond spatial pyramids: A new feature extraction framework with dense spatial sampling for image classification," in *ECCV*, 2012.
- [33] M. Jain, H. Jegou, and P. Bouthemy, "Better exploiting motion for better action recognition," in *CVPR*, 2013.
- [34] M. Jain, J. van Gemert, H. Jegou, P. Bouthemy, and C. G. Snoek, "Action localization with tubelets from motion," in *CVPR*, 2014.
- [35] D. Oneata, J. Verbeek, and C. Schmid, "Efficient action localization with approximately normalized fisher vectors," in *CVPR*, 2014.
- [36] H. Wang and C. Schmid, "Action recognition with improved trajectories," in *ICCV*, 2013.
- [37] I. Laptev, M. Marszalek, C. Schmid, and B. Rozenfeld, "Learning realistic human actions from movies," in *CVPR*, 2008.
- [38] K. Simonyan and A. Zisserman, "Two-stream convolutional networks for action recognition in videos," in *NIPS*, 2014.
- [39] R. Fergus, P. Perona, and A. Zisserman, "Weakly supervised scale-invariant learning of models for visual recognition," *IJCV*, vol. 71, no. 3, pp. 273–303, March 2007.
- [40] C. Desai and D. Ramanan, "Detecting actions, poses, and objects with relational phraselets," in *ECCV*, 2012.
- [41] Y. Yang and D. Ramanan, "Articulated pose estimation with flexible mixtures-of-parts," in *CVPR*, 2011.
- [42] X. Zhu and D. Ramanan, "Face detection, pose estimation, and landmark localization in the wild," in *CVPR*, 2012.
- [43] X. Zhu, C. Vondrick, D. Ramanan, and C. Fowlkes, "Do we need more training data or better models for object detection?" in *BMVC*, 2012.
- [44] L. Bourdev, S. Maji, and J. Malik, "Describing people: Poselet-based attribute classification," in *ICCV*, 2011.
- [45] —, "Describing people: A poselet-based approach to attribute classification," in *ICCV*, 2011.
- [46] L. Bourdev and J. Malik, "Poselets: Body part detectors trained using 3D human pose annotations," in *ICCV*, 2009.
- [47] S. Maji, L. Bourdev, and J. Malik, "Action recognition from a distributed representation of pose and appearance," in *CVPR*, 2011.
- [48] Y.-L. Boureau, F. Bach, Y. LeCun, and J. Ponce, "Learning mid-level features for recognition," in *CVPR*, 2010.
- [49] A. Fathi and G. Mori, "Action recognition by learning mid-level motion features," in *CVPR*, 2008.
- [50] J. Joo, S. Wang, and S.-C. Zhu, "Human attribute recognition by rich appearance dictionary," in *ICCV*, 2013.
- [51] M. Juneja, A. Vedaldi, C. Jawahar, and A. Zisserman, "Blocks that shout: Distinctive parts for scene classification," in *CVPR*, 2013.
- [52] J. J. Lim, C. L. Zitnick, and P. Dollár, "Sketch tokens: A learned mid-level representation for contour and object detection," in *CVPR*, 2013.
- [53] M. Oquab, L. Bottou, I. Laptev, and J. Sivic, "Learning and transferring mid-level image representations using convolutional neural networks," in *CVPR*, 2014.
- [54] P. Szabzmeydani and G. Mori, "Detecting pedestrians by learning shapelet features," in *CVPR*, 2007.
- [55] S. Singh, A. Gupta, and A. Efros, "Unsupervised discovery of mid-level discriminative patches," *ECCV*, 2012.
- [56] J. Sun and J. Ponce, "Learning discriminative part detectors for image classification and cosegmentation," in *ICCV*, 2013.
- [57] B. Yao, X. Jiang, A. Khosla, A. L. Lin, L. J. Guibas, and L. Fei-Fei, "Action recognition by learning bases of action attributes and parts," in *ICCV*, 2011.
- [58] S. N. Parizi, A. Vedaldi, A. Zisserman, and P. Felzenszwalb, "Automatic discovery and optimization of parts for image classification," in *ICLR*, 2015.
- [59] O. Boiman and M. Irani, "Similarity by composition," in *NIPS*, 2006.
- [60] B. Leibe, A. Leonardis, and B. Schiele, "Robust object detection with interleaved categorization and segmentation," *IJCV*, vol. 77, no. 1, pp. 259–289, 2008.
- [61] O. Boiman, E. Shechtman, and M. Irani, "In defense of nearest-neighbor based image classification," in *CVPR*, 2008.
- [62] P. Zhu, L. Zhang, Q. Hu, and S. Shiu, "Multi-scale patch based collaborative representation for face recognition with margin distribution optimization," in *ECCV*, 2012.
- [63] T. Guha and R. K. Ward, "Learning sparse representations for human action recognition," *PAMI*, vol. 34, no. 8, pp. 1576–1588, 2012.
- [64] M. Andriluka, L. Pishchulin, P. Gehler, and B. Schiele, "2D human pose estimation: New benchmark and state of the art analysis," in *CVPR*, 2014.
- [65] J. Charles, T. Pfister, M. Everingham, and A. Zisserman, "Automatic and efficient human pose estimation for sign language videos," *IJCV*, vol. 110, no. 1, pp. 70–90, 2014.
- [66] M. Dantone, J. Gall, C. Leistner, and L. Van Gool, "Body parts dependent joint regressors for human pose estimation in still images," *PAMI*, vol. 36, no. 11, pp. 2131–2143, 2014.
- [67] X. Fan, K. Zheng, Y. Lin, and S. Wang, "Combining local appearance and holistic view: Dual-source deep neural networks for human pose estimation," in *CVPR*, 2015.
- [68] J. J. Tompson, A. Jain, Y. LeCun, and C. Bregler, "Joint training of a convolutional network and a graphical model for human pose estimation," in *NIPS*, 2014.
- [69] A. Toshev and C. Szegedy, "DeepPose: Human pose estimation via deep neural networks," in *CVPR*, 2014.

- [70] R. Vemulapalli, F. Arrate, and R. Chellappa, "Human action recognition by representing 3D skeletons as points in a lie group," in *CVPR*, 2014.
- [71] C. Thureau and V. Hlavac, "Pose primitive based human action recognition in videos or still images," in *CVPR*, 2008.
- [72] H. Chen, A. Gallagher, and B. Girod, "Describing clothing by semantic attributes," in *ECCV*, 2012.
- [73] B. Yao and L. Fei-Fei, "Action recognition with exemplar based 2.5D graph matching," in *ECCV*, 2012.
- [74] N. Zhang, M. Paluri, M. Ranzato, T. Darrell, and L. Bourdev, "Panda: Pose aligned networks for deep attribute modeling," in *CVPR*, 2014.
- [75] S. Ma, S. Sclaroff, and N. Ikizler-Cinbis, "Unsupervised learning of discriminative relative visual attributes," in *ECCV Workshops*, 2012.
- [76] N. Kumar, A. C. Berg, P. N. Belhumeur, and S. K. Nayar, "Describable visual attributes for face verification and image search," *PAMI*, vol. 33, no. 10, pp. 1962–1977, 2011.
- [77] O. Rudovic, M. Pantic, and I. Patras, "Coupled gaussian processes for pose-invariant facial expression recognition," *PAMI*, vol. 35, no. 6, pp. 1357–1369, 2013.
- [78] G. Sharma, S. ul Hussain, and F. Jurie, "Local higher-order statistics (LHS) for texture categorization and facial analysis," in *ECCV*, 2012.
- [79] S. Wan and J. Aggarwal, "Spontaneous facial expression recognition: A robust metric learning approach," *PR*, vol. 47, no. 5, pp. 1859–1868, 2014.
- [80] C. Li, Q. Liu, J. Liu, and H. Lu, "Learning ordinal discriminative features for age estimation," in *CVPR*, 2012.
- [81] K.-Y. Chang and C.-S. Chen, "A learning framework for age rank estimation based on face images with scattering transform," *TIP*, vol. 24, no. 3, pp. 785–798, 2015.
- [82] X. Geng, Z.-H. Zhou, and K. Smith-Miles, "Automatic age estimation based on facial aging patterns," *PAMI*, vol. 29, no. 12, pp. 2234–2240, 2007.
- [83] G. Guo, G. Mu, Y. Fu, C. Dyer, and T. Huang, "A study on automatic age estimation using a large database," in *ICCV*, 2009.
- [84] G. Guo and X. Wang, "A study on human age estimation under facial expression changes," in *CVPR*, 2012.
- [85] M. Shao, L. Li, and Y. Fu, "What do you do? occupation recognition in a photo via social context," in *ICCV*, 2013.
- [86] G. Guo and A. Lai, "A survey on still image based human action recognition," *PR*, vol. 47, no. 10, pp. 3343–3361, 2014.
- [87] S. Hussain and B. Triggs, "Feature sets and dimensionality reduction for visual object detection," in *BMVC*, 2010.
- [88] F. Perronnin, Z. Akata, Z. Harchaoui, and C. Schmid, "Towards good practice in large-scale learning for image classification," in *CVPR*, 2012.
- [89] A. Oliva and A. Torralba, "Modeling the shape of the scene: A holistic representation of the spatial envelope," *IJCV*, vol. 42, pp. 145–175, 2001.
- [90] A. Krizhevsky, I. Sutskever, and G. E. Hinton, "Imagenet classification with deep convolutional neural networks," in *NIPS*, 2012.
- [91] F. Porikli, "Integral histogram: A fast way to extract histograms in cartesian spaces," in *CVPR*, 2005.
- [92] F. C. Crow, "Summed-area tables for texture mapping," *SIG-GRAPH*, vol. 18, no. 3, pp. 207–212, 1984.
- [93] P. Viola and M. Jones, "Robust real-time object detection," *IJCV*, vol. 4, pp. 51–52, 2001.
- [94] H. Bay, A. Ess, T. Tuytelaars, and L. V. Gool, "SURF: Speeded up robust features," *CVIU*, vol. 110, no. 3, pp. 346–359, 2008.
- [95] O. Veksler, "Fast variable window for stereo correspondence using integral images," in *CVPR*, 2003.
- [96] A. Adam, E. Rivlin, and I. Shimshoni, "Robust fragments-based tracking using the integral histogram," in *CVPR*, 2006.
- [97] A. Vedaldi and B. Fulkerson, "VLFeat: An open and portable library of computer vision algorithms," <http://www.vlfeat.org/>, 2008.
- [98] A. Vedaldi and A. Zisserman, "Efficient additive kernels using explicit feature maps," in *CVPR*, 2010.
- [99] R.-E. Fan, K.-W. Chang, C.-J. Hsieh, X.-R. Wang, and C.-J. Lin, "LIBLINEAR: A library for large linear classification," *JMLR*, vol. 9, pp. 1871–1874, 2008.
- [100] K. Simonyan and A. Zisserman, "Very deep convolutional networks for large-scale image recognition," *ICLR*, 2015.
- [101] C. Szegedy, W. Liu, Y. Jia, P. Sermanet, S. Reed, D. Anguelov, D. Erhan, V. Vanhoucke, and A. Rabinovich, "Going deeper with convolutions," in *CVPR*, 2015.
- [102] P. Sermanet, K. Kavukcuoglu, S. Chintala, and Y. LeCun, "Pedestrian detection with unsupervised multi-stage feature learning," in *CVPR*, 2013.
- [103] R. Girshick, J. Donahue, T. Darrell, and J. Malik, "Rich feature hierarchies for accurate object detection and semantic segmentation," in *CVPR*, 2014.
- [104] S. Ji, W. Xu, M. Yang, and K. Yu, "3D convolutional neural networks for human action recognition," *PAMI*, vol. 35, no. 1, pp. 221–231, 2013.
- [105] J. Deng, W. Dong, R. Socher, L.-J. Li, K. Li, and L. Fei-Fei, "Imagenet: A large-scale hierarchical image database," in *CVPR*, 2009.
- [106] A. S. Razavian, H. Azizpour, J. Sullivan, and S. Carlsson, "Cnn features off-the-shelf: an astounding baseline for recognition," in *CVPR*, 2014.
- [107] A. Vedaldi and K. Lenc, "Matconvnet – convolutional neural networks for matlab," *arXiv*, 2014.
- [108] L. Li, H. Su, E. Xing, and L. Fei-Fei, "Object bank: A high-level image representation for scene classification and semantic feature sparsification," in *NIPS*, 2010.
- [109] J. Wang, J. Yang, K. Yu, F. Lv, T. Huang, and Y. Gong, "Locality-constrained linear coding for image classification," in *CVPR*, 2010.



**Gaurav Sharma** is currently with the Max Planck Institute for Informatics, Germany. He holds an Integrated M.Tech. (5 years programme) in Mathematics and Computing from the Indian Institute of Technology Delhi (IIT Delhi), India and a PhD in Applied Computer Science from INRIA (LEAR team) and GREYC – CNRS UMR6072, University of Caen, France. His primary research interest lies in Computer Vision and applied Machine Learning.



**Frédéric Jurie** is a professor at the Université de Caen Basse-Normandie, France (GREYC – CNRS UMR6072). His research interests lie predominantly in the area of Computer Vision, particularly with respect to object recognition, image classification and object detection.



**Cordelia Schmid** holds a M.S. degree from the University of Karlsruhe and a Doctorate from the Institut National Polytechnique de Grenoble (INPG). She is a research director at INRIA, France, and directs the team LEAR. She is the author of over a hundred technical publications. She was awarded the Longuet-Higgins prize for fundamental contributions in computer vision that have withstood the test of time twice in 2006 & 2014, an ERC advanced grant in 2012 and Humboldt prize in 2015. She is a fellow of IEEE.